EIGHTEENTH EUROPEAN ROTORCRAFT FORUM

Paper N° 108

UNSTEADY FREE WAKE ANALYSIS OF CLOSELY INTERFERING HELICOPTER ROTORS

A.BARON, M.BOFFADOSSI

Dipartimento di Ingegneria Aerospaziale
del Politecnico di Milano
Via C.Golgi, 40 - 20133 Milano - Italy

September 15-18, 1992
AVIGNON, FRANCE

This paper has been presented during ERF 1992 Technical Sessions in Avignon, France.
The written original document has been lost, so it has not been included in the 1992 proceedings or distributed during the Forum.

ASSOCIATION AERONAUTIQUE ET ASTRONAUTIQUE DE FRANCE

Unsteady Free Wake Analysis of Closely Interfering Helicopter Rotors

A.Baron, M.Boffadossi

Dipartimento di Ingegneria Aerospaziale del Politecnico di Milano
Via C. Golgi, 40 - 20133 Milano - Italy

Abstract

A non-linear unsteady vortex lattice scheme has been developed for the simulation of the flow past closely interfering helicopter rotors in general unsteady motion.
It has been applied satisfactorily to a variety of impulsively started multi-rotor configurations and proved to be capable to predict flowfield and load distribution on the rotor blades, without recourse to any form of tuning of the free wake model.
A time evolution of the viscous cores of the discrete Rankine vortices is imposed using a turbulent diffusion model physically consistent with the diffusion process of the continuous turbulent shear layers.

1 - Introduction

The distribution of vorticity past helicopter rotors depends on various factors, such as the flight and load condition, the number and geometry of the blades, etc. Among these factors, the mutual location and aerodynamic interference of the rotors can also strongly affect the development of the wakes and the instantaneous vorticity field in the vicinity of the blades. As a consequence, the instantaneous load distribution on the rotor blades is also affected.

Single rotor helicopters use an auxiliary tail rotor to provide torque balance and yaw control, while twin rotor configurations adopt counter-rotating rotors, having approximately the same size and loading, arranged in coaxial, tandem or side-by-side configurations (Johnson, 1980).
In all of these cases, rotors are either overlapping or closely arranged so that both instantaneous flowfield and loads are dominated by the non-linear effects associated with the mutual induction of the lifting surfaces and the vortical wakes shed in the field.

These non linear phenomena play a dominant role in the aerodynamic design of rotorcrafts. This is why accurate predictions of stability, performances, vibrations, aeroelastic behavior and noise generated by rotor blades are strictly related to the ability in predicting the instantaneous strength, structure and location of the closely interfering wakes (Johnson, 1990).

2 - Vorticity field past helicopter rotors

Helicopter rotors are characterized by high aspect-ratio blades trailing vorticity into the wake. Vorticity remains mainly confined in the tip vortices originated by the intense roll-up of the continuous wakes released at trailing edges, so that the wake consists of concentrated tip vortices trailed in skewed interlocking and distorting helices.
In hover flight, convection of vorticity is only produced by the self-induced velocities of the wakes. In forward flight, the helical tip vortices are still subject to mutual induction, but are also convected rearward, as well as downward, by the effect of the relative velocity of the helicopter with respect to the atmosphere (see Landgrebe and Cheney, 1972).

In the last fifteen years, many numerical methods and free wake schemes have been developed aimed at predicting aerodynamic loads and configuration of the wakes past helicopter rotors. However, most of the work concerned single isolated rotors in hover or steady forward flight (Summa and Maskew, 1981; Rosen and Graber, 1988; Felker et al., 1990).
Only minor advances have been recently obtained in the simulation capabilities of unsteady flight regimes and limited attention has been devoted to the complex interaction of the main rotor wake with fuselages, empennages and tail rotors.

When dealing with multi rotor configurations, the flow conditions encountered by each single blade are non uniform, even in steady flight regimes (e.g. hovering), and complex interactional aerodynamics cannot be neglected.

In the present work an unsteady vortex-lattice scheme is presented, which has been satisfactorily applied to a variety of multi rotor configurations and proved to be capable to predict flowfield and load distribution on the blades of closely interfering impulsively started rotors, without recourse to any form of tuning of the free wake model.

With a time dependent approach, not only the need for an initial guess of the wakes is eliminated, but general unsteady maneuvers can also be easily simulated, by simply considering the actual time dependent boundary conditions which represent, at each time step, the instantaneous velocity and attitude of each single rotor blade.

3 - The computational method

On the basis of a non linear vortex lattice scheme (Baron and Boffadossi, 1991) developed to model the unsteady incompressible flow past isolated rotors of arbitrary geometry, a code for the prediction of wake configurations and load distributions on closely interfering and overlapping rotors has been derived.

The basic assumptions, capabilities and limitations of the method are briefly summarized in the following.

Blades are assumed to have negligible thickness and are simulated as rigid, plane or cambered surfaces with arbitrary twist and taper distribution.
They can undergo general independent unsteady motions, including flapping and pitching effects.

Wakes can be released in the flowfield from any of the sharp edges of the blades, depending on their planform, aspect ratio and attitude.

Geometry of the wakes and distribution of the aerodynamic loads are predicted, as a function of time, starting from an initial state of rest.

The code can treat general multiple rotor configurations and blade planforms, provided that the lines along which wake separation takes place (regardless of their number and location) are assigned "a priori".

The unsteady flow of an incompressible ideal fluid is irrotational in the region outside the lifting surfaces and the separated vortex sheets. It is therefore governed by Laplace's equation:

$$\nabla^2\phi(\mathbf{R},t)=0 \tag{3.1}$$

where ϕ is the velocity potential at time t, expressed in terms of the absolute position vector $\mathbf{R}$.

The second order, linear differential equation (3.1) can be solved once appropriate boundary conditions are prescribed at any time t. These satisfy the far field condition ($\nabla\phi=0$, $\mathbf{R}=\infty$) and the no-penetration condition on the material surfaces S_B:

$$[\nabla\phi(\mathbf{R},t) - \mathbf{V}^B(\mathbf{R},t)] \cdot \mathbf{n}(\mathbf{R},t) = 0 \qquad \text{on } S_B \tag{3.2}$$

where $\mathbf{V}^B(\mathbf{R},t)$ is the local body velocity vector and $\mathbf{n}(\mathbf{R},t)$ is the local unit vector normal to the surface.
In addition, when flight in ground effect has to be simulated, the no-penetration condition on the ground surface is also imposed by using the virtual image technique.

For the solution of equation (3.1), the Green's theorem is used and blades and wakes are discretized into a finite number of surface panels with constant doublet strength $\mu = \Delta\phi$. Due to the equivalence between doublet and vorticity distributions (Hoeijmakers, 1989), each panel is therefore made up of straight vortex segments lying on its perimeter, forming a closed loop of circulation $\Gamma=\Delta\phi$ (Mook, 1988).

The unknown values of the N circulations $\Gamma(t)_i$ on the lifting surface panels are determined, at each time step, imposing the zero normal velocity condition (3.2) on the panel control points. Velocities are evaluated at control points through the Biot-Savart law.

The following linear system of N algebraic equations must then be solved at each time t:

$$\sum_{j=1}^{N} A(t)_{ij}\ \Gamma(t)_j = \left[\mathbf{V}^B(t)\cdot\mathbf{n}(t)\right]_i - \left[\mathbf{V}^{SW}(t-\Delta t)\cdot\mathbf{n}(t)\right]_i \qquad (i=1,N) \tag{3.3}$$

where:

$A(t)_{i,j}=(\mathbf{V}_j^{SB}\cdot\mathbf{n})_i$ is the normal component of the velocity induced, at time t, in the control point of the i-th panel by a unit circulation lying on the j-th panel;

$\Gamma(t)_j$ is the circulation on the j-th panel, at time t;

$\mathbf{V}^{B}(t)_i$ is the velocity of the control point of the i-th panel ensuing from the unsteady motion of the lifting surface;

$\mathbf{V}^{SW}(t-\Delta t)_i$ is the velocity induced by the wakes on the control point of the i-th panel at time $(t-\Delta t)$, which, at time t=0, is assumed equal to zero, consistently with the hypothesis of impulsive start;

$\mathbf{n}(t)_i$ is the unit vector normal to the i-th panel, at time t.

Starting from the rest, wakes are generated in a Lagrangian process, by releasing in the field the vorticity present on the edge panels of the blades. At the instant motion begins no vorticity has been convected, so no wakes exist but a starting vortex forms along the sharp edges and is subsequently shed into the field.
To obtain this, panels from the edges along which vorticity is shed are "moved" into the field and form a first row of wake panels. At the following time steps, each node of the existing wake is convected to a new position and a new row of panels is added to the wakes.

In order to produce force free vortical sheets, the instantaneous local velocity is computed and used to displace the nodes of the wakes, adopting a second order Adams-Bashforth scheme.

According to Kelvin's theorem, vorticity is conserved and circulation around each vortex segment in the wakes remains constant.

The distribution of the net pressure coefficient on the lifting surfaces is calculated by using Bernoulli's unsteady equation, written in a blade fixed frame of reference (Kandil, 1985). Total load coefficients are obtained by integration of pressure distributions.

4 - Definition of the frames of reference

In order to determine the coefficients of the aerodynamic influence matrix $[A(t)]$, the instantaneous location and attitude of each blade element in the absolute frame of reference, must be computed.

Moreover the velocity of the control point of each blade panel must be prescribed. This is the result of flapping, pitching and rotation of the blades around the correspondent rotors axes, and of both linear and angular velocities of the rotorcraft (offset of the hinges and lag motion of the blades are neglected in the present formulation).

At time t, the relative position vector $\mathbf{r}_P(t)_i$ of a generic point P laying on the k-th blade of the i-th rotor, in the local non rotating frame of reference having the origin in the hub of the i-th rotor H_i, can be expressed as a function of its initial position P_0:

$$\mathbf{r}_P(t)_i = \mathcal{R}_k(t)_i \, (P_0 - H_{0i}) \tag{4.1}$$

where H_{0i}, indicates the position of the rotor hub at time t=0, and $\mathcal{R}_k(t)_i$ is the tensor associated with the rotation of the k-th blade, with respect to the initial values of azimuthal, flapping and pitching angles. $\mathcal{R}_k(t)_i$ therefore includes the instantaneous contributions of the azimuthal angle $\psi_k(t)_i$, the flapping angle $\beta_k(t)_i$ and the pitching angle $\vartheta_k(t)_i$, of the k-th blade, defined

by:

$$\psi_k(t)_i = \Omega_i t + 2\pi(k-1)/n \tag{4.2}$$

$$\beta_k(t)_i = \beta_c(t)_i - \beta_1(t)_i \cos \psi_k(t)_i - \beta_2(t)_i \sin \psi_k(t)_i \tag{4.3}$$

$$\vartheta_k(t)_i = \vartheta_c(t)_i - \vartheta_1(t)_i \cos \psi_k(t)_i - \vartheta_2(t)_i \sin \psi_k(t)_i \tag{4.4}$$

where Ω_i denotes the rotational speed of the i-th rotor.

The absolute position vector $\mathbf{R}_P(t)$ of the point P, can be expressed by:

$$\mathbf{R}_P(t) = \mathcal{R}(t)(\mathbf{r}_P(t)_i + \mathbf{r}_{Hi}) + \mathbf{R}_G(t) \tag{4.5}$$

where $\mathbf{r}_{Hi}$=H-G, denotes the relative position of the rotor hub H_i with respect to the helicopter center of gravity G, of which $\mathbf{R}_G(t)$ is the absolute position at time t.
$\mathcal{R}(t)$ is the tensor associated with the rotation of the helicopter with respect to its orientation in the initial state of rest (t=0).
Therefore, at time t, the absolute velocity of a generic point P laying on the k-th blade of the i-th rotor can be determined according to:

$$\mathbf{V}_P(t) = \mathbf{v}_P(t)_i + \mathbf{W}(t) \wedge (\mathbf{R}_P(t) - \mathbf{R}_G(t)) + \mathbf{V}_G \tag{4.6}$$

$\mathbf{W}(t)$ is the instantaneous maneuvering angular velocity of the helicopter, $\mathbf{V}_G$ is the linear velocity of its center of gravity, and $\mathbf{v}(t)_i$ is the local velocity of point P consequent to the rotational speed of the rotor, and blade flapping and pitching motions:

$$\mathbf{v}_P(t)_i = \mathbf{w}_k(t)_i \wedge \mathbf{r}_P(t)_i \tag{4.7}$$

where $\mathbf{w}_P(t)_i$ is the instantaneous angular velocity of the k-th blade, consequent to rotational speed of the i-th rotor, and flapping and pitching motions of the k-th blade.

5 - Vortex modeling

Vortex filaments are extremely efficient from a computational point of view and their use is in practice compulsory when iterative or time marching schemes have to be used. Nevertheless, they introduce in the flowfield lines along which, according to the Biot-Savart law, the induced velocity tends to infinity. The singular behavior of vortex filaments can be such to produce numerical instabilities and may cause the solution to diverge.

This problem can be eliminated by preventing the induced velocity, at points close to the vortex axes, from increasing above a certain value. This can be done in a variety of ways and basically consists in introducing what is called a vortex, or vortex core, model.
In the present work Rankine vortices are used and a viscous core diffusion model physically consistent with the turbulent diffusion mechanism of continuous shear layers (Baron et al., 1990). While avoiding the recourse to any explicit modeling of the tip vortices, it allows to cope, without any form of tuning, even with the rapid roll-up process of unsteady interfering wakes.

Rankine vortices are assumed to be "equivalent" to the elementary portions of the physically continuous shear layers they replace in the numerical scheme.

Therefore, their core radii spread in such a way that their cross sectional area S and circulation $\Gamma=\gamma\ell$ are equal, at each time, to spreading and circulation of an elementary portion of continuous shear layer containing the same vorticity.
This implies a rate of change of their radius r_c given by:

$$\frac{dr_c}{dt} = \frac{K\,\Gamma}{2\pi r_c} \tag{5.1}$$

where the diffusion constant K, both for forced and unforced turbulent shear layers, assumes a universal value equal to 0.095, as demonstrated by experimental evidence (Liepmann and Laufer 1947; Brown and Roshko, 1974; Oster and Wygnanski, 1982; Lesieur, 1987).
Equation (5.1) is used to model the core diffusion process of each Rankine vortex in the vortex lattice scheme.

Note that most commonly used vortex core diffusion models turn out to be strongly dependent on the number of vortex filaments used to discretize the continuous distribution of vorticity in the flowfield. The present approach, on the contrary, is virtually independent on discretization, the turbulent diffusion being explicitly related to the circulation of each vortex filament and, therefore, to the number of vortices.
This brings to a kind of "self adaptation" of the model and explains why, in a variety of applications, no tuning has been required for a correct simulation of the vortex core diffusion.

6 - Numerical results

Some applications of the unsteady vortex lattice scheme are examined in the following, aimed at illustrating the capabilities of the code.
Although the code can treat general unsteady motions of multi rotor configurations, only impulsive starts in hover flight are here presented. This allows to compare the numerical predictions with available steady state experimental measurements.
Moreover, the main purpose of the present investigation is to assess the capability of relatively simple schemes to manage complex interactional aerodynamics, rather than to compute complex flowfields past realistic helicopter configurations.

Turbulent diffusion of the cores of the discrete vortices is modeled according to equation (5.1), which involves neither tuning nor choice of numerical parameters.

Refinement of the geometrical discretization of the lifting surfaces obviously brings to an increasingly better definition of the load distribution on the rotor blades, but also requires rapidly growing computing times.
A preliminary analysis of the sensitivity of the scheme to panel density has shown that, for rotor blades having rectangular planforms and relatively high aspect-ratio, an accurate prediction of the aerodynamic loads can be obtained even by using a limited number of vortex panels: typically 4 by 6 panels, in chordwise and spanwise directions. Solutions are only negligibly improved by further increase of the number of panels.

Flowfield and aerodynamic load on rotor blades rely upon the instantaneous location of the shed wakes. Therefore, an appropriate integration time step must be used to accurately evaluate the displacement of the nodes of the vortex

lattice. Moreover, the time discretization also affects the longitudinal dimension of the vortex panels in the wake, so influencing the uniformity of the vortex elements. Though not strictly compulsory, time discretization should be such to produce nearly uniform vortex elements on wakes and lifting surfaces. These are known to increase accuracy of the solutions and stability of the numerical scheme.
All the numerical results presented in the following have been obtained using a dimensionless integration time step equivalent to 1/32 of rotor revolution. This value meets rather well the antithetical requirements of accuracy and computing time.

6.1 - Two-bladed main rotor/tail rotor configuration

In order to analyze the effect of rotor/rotor interference, a comparison is made between the behavior of a rotor of given geometry when isolated or part of a typical main rotor/tail rotor configuration.
This is an example of a relatively simple case in which, however, traditional numerical techniques based on prescribed (Kocurek and Tangler, 1977) or relaxed free wakes (Rosen and Graber, 1988) prove to be useless and recourse must be done to unsteady free wake models .

In order to compare the numerical results obtained for the isolated case with the experimental steady state measurements by Caradonna and Tung (1981), two-bladed rotors have been selected with constant chord, aspect ratio equal to 6 and collective pitch of 8 degrees. The same geometry, scaled down of a factor 3, and the same collective pitch are used for the tail rotor. The tail rotor has its rotation axis laying in the main rotor disk plane, at a distance Dx from the main rotor axis varying from 1.4 to 2.2 main rotor radii R.

For Dx=1.4R, the time evolution of the wake, consequent to an impulsive start, is reported in **Fig.2**, after 1, 3 and 10 rotor revolutions. Note that in the representation of the wakes the thickness of the lines identifying the vortical filaments is proportional to the circulation of each filament. Only the wake of a single blade per rotor is shown for clarity.
It is interesting to note how the tail rotor wake is progressively captured by the main rotor's one, and how strongly it is distorted.

The time evolution of the rotor thrust coefficient is reported in **Fig.1**. For the isolated rotor case (also see Baron and Boffadossi, 1991), thrust rapidly increases in the initial stage of the impulsive start, until each blade interacts with the starting vortex shed in the field by the preceding one. Then, due to the development of a self-induced velocity field, the thrust coefficient progressively reduces and exactly matches the steady state measured value (Caradonna and Tung, 1981).

For the interfering case, the main rotor thrust shows to be but weakly reduced, while the tail rotor flowfield is strongly affected by the periodic induction of the main rotor blades.
The tail rotor is therefore subject to significant oscillatory loads, not only in the initial stage of the impulsive start (the first 4 rotor revolutions) but even when an approximately steady state condition is attained, and it produces a thrust coefficient higher than the isolated rotor. In this configuration significant vibration levels and fatigue loads can be produced, and although not included in the present formulation, also the torque exerted by the tail rotor will be periodically affected during each rotation, so inducing possible coupled vibrations.

Higher thrust coefficients can be explained by the a reduced axial development of the tail rotor wake, caused by the main rotor suction, which produces lower induced velocities through the tail rotor disk.

In order to examine the effects of the main rotor/tail rotor interference, the longitudinal distance Dx between the rotor axes has been increased to 1.8 and 2.2 main rotor radii. The tail rotor axis still lays in the main rotor disk plane.

In **Fig.3** the time evolution of the wakes is shown for Dx=1.8 and 2.2 main rotor radii, after 10 rotor revolutions.
For Dx=1.8R, the tail rotor wake is still captured in the main rotor one, but interference is weaker. It is worth to note the formation of a distorted vortex ring collecting the tail rotor blade tip vortex filaments. This vortex ring, in its lower part is completely rolled-up in the main rotor wake, while its upper portion is only affected by the overall main rotor induction.
For Dx=2.2R, the tail rotor wake develops along its own axis, the two wakes remain completely apart and their geometry is quite similar.

The effect of the separation distance between the rotor axes on the thrust coefficient of the main rotor and tail rotor blades is clearly evident in **Fig.4**.
Even at steady state, when the rotors are relatively close each other, sharp peaks are present in the main rotor blade thrust, caused by the periodic interference of the blade tips with the tail rotor wake. Only for Dx=2.2R the time evolution of the thrust coefficient of the main rotor blades becomes relatively smooth.
Oscillatory loads are definitely stronger on the tail rotor blades and their amplitude remains still significant even for the larger value of the separation distance Dx.

6.2 - Coaxial rotor configuration

An helicopter configuration based on a couple of counter-rotating coaxial rotors is also considered. The geometry of the rotors is the same as the previous case and three different vertical separation distances Dz between the rotor disk planes are considered, equal to 0.05, 0.10 and 0.30 rotor radii, in order to determine its effect.

In **Fig. 5** the configuration of the wake is shown, after 8 rotor revolutions, for Dz=0.1R. Note how the tip vortex filaments, in particular the ones produced by the upper rotor, are strongly distorted, because of the close interaction of the blades. This produces again oscillatory loads, the amplitude of which is larger for the blades of the lower rotor, as reported in **Fig.6**.

In **Fig. 6**, thrust shows to be but negligibly affected by the coaxial arrangement during the initial stage consequent to the impulsive start, namely until the wakes shed in the field remain practically confined in the rotor disk planes.
Then, due to the development of a self-induced velocity field, thrust coefficients progressively reduce. Only at this stage the influence of the vertical spacing of the rotors becomes significant in affecting both the mean and the instantaneous values of the blade thrust.
Increasing the separation between the rotor disk planes obviously brings to a reduced amplitude of the mutually induced oscillatory loads, however enhances the difference in the thrust produced by the two rotors.

6.3 - Tandem rotor configuration

Finally, a tandem twin rotor configuration is considered. Each rotor has three blades having the same geometry of the previous cases.
The horizontal distance Dx between the rotor axis is equal to 1.3 rotor radii, while their vertical separation is 0.13R, the front rotor being located below the rear one.

In **Fig.7**, a 2-D vector plot of the instantaneous velocity field in the wake is shown, in a vertical plane containing the rotor axes, after 1 3, and 10 rotor revolutions after the impulsive start.
Blade tip vortices appear first, which progressively grow and are convected downstream by the self-induced velocity field, forming a toroidal starting vortex. The overlapping of the two rotors produces higher induced velocities in the inner part of the wake and consequently the contraction of the wake appears to be enhanced.

In **Fig.8** the time evolution of the blade thrust coefficient is reported. Note how the thrust coefficient rapidly tends to an oscillatory behavior with constant amplitude and frequency. However, due to the mutual location of the rotors, induction effects are much more significant on the blades of the front lower rotor, which partially lays in the wake of the rear one.

7 - Conclusions

A non-linear unsteady vortex lattice scheme has been developed for the simulation of the flow past closely interfering helicopter rotors in general unsteady motion.

It has been applied satisfactorily to a variety of multi-rotor configurations impulsively started in hover flight and proved to be capable to compute the instantaneous flowfield and load distribution on the rotor blades, without recourse to any form of tuning of the free wake model.

The capability of predicting the time evolution of closely interfering unsteady wakes is probably ascribable to the use of a physically consistent model for the turbulent diffusion of the viscous cores of the discrete Rankine vortices.

It has been evidenced that interfering rotors affect their behavior not only through a mutually induced velocity field, but mainly through non linear local distortions of their wakes.

All of the examined configurations proved to be strongly affected by the mutual interference of the rotors. As a result, even in steady state flight regimes, the instantaneous values of the aerodynamic loads can be such to produce significant vibration levels and fatigue loads. However, both of them, together with the mean value of the produced thrust, can be deeply modified by selecting an appropriate mutual location of the rotors.

Acknowledgments

This work has been partially supported during 1991 by the Ministero dell'Universita' e della Ricerca Scientifica e Tecnologica.

List of symbols

AR	blade aspect-ratio, $(R-r_0)/C$
C	mean blade chord
C_T	rotor thrust coeff., $T/\rho(\Omega R)^2\pi R^2$
Dx	longitudinal separation of the rotor axes
Dz	vertical separation of the rotor disk planes
K	constant in the vortex core turbulent diffusion model
ℓ	spanwise dimension of the elementary portion of shear layer
n	local unit vector normal to the blade surface
N	number of vortex panels on the blades
r_c	vortex core radius
r	relative position vector
R	blade tip radius
R	absolute position vector
$\mathcal{R}$	rotation tensor
t	time
t_c	characteristic time, $2\pi/\Omega$
t	dimensionless time, t/t_c
T	rotor thrust
v	relative velocity
V	absolute velocity
w	relative angular velocity
W	absolute angular velocity
β	blade flap angle (positive upward)
β_c	coning angle
β_1	longitudinal flap angle
β_2	lateral flap angle
ϕ	velocity potential
γ	linear vortex density vector
Γ	circulation; vortex strength
μ	doublet strength
ρ	air density
ϑ	pitch angle
ϑ_c	collective pitch angle
ϑ_1	longitudinal pitch angle
ϑ_2	lateral pitch angle
ψ	rotor blade azimuth angle
Ω	rotor rotational speed

Subscripts and superscripts:

B	blade
G	center of gravity
H	rotor hub
i	index of generic rotor
k	index of generic blade
o	initial state
S_B	blade surface
S_W	wake surface

References

BARON A., BOFFADOSSI M., DE PONTE S. (1990), Numerical simulation of vortex flows past impulsively started wings, AGARD-CP-494, paper N.33.

BARON A., BOFFADOSSI M. (1991), Numerical simulation of unsteady rotor wakes, 17-th European Rotorcraft Forum, Berlin.

BROWN G.L., ROSHKO A. (1974), On density effects and large structure in turbulent mixing layers, J.Fl.Mech., Vol.64, pp. 775-816.

CARADONNA F.X., TUNG C. (1981), Experimental and analytical studies of a model helicopter rotor in hover, Vertica, Vol.5, N.2, pp.149-161.

FELKER F.F., QUACKENBUSH T.R., BLISS D.B., LIGHT J.S. (1990) , Comparison of predicted and measured rotor performance in hover using a new free wake analysis, Vertica, Vol.14, N.3, pp.361-383.

HOEIJMAKERS H.W.M. (1989), Computational vortex flows aerodynamics, AGARD CP 342.

JOHNSON W. (1980), Helicopter Theory, Princeton University Press.

JOHNSON W. (1990), Airloads and Wake Models for a Comprehensive Helicopter Analysis, Vertica, Vol.14, N.3, pp.255-300.

KANDIL, O.A. (1985), Steady and unsteady incompressible free-wake analysis, in "Computational Methods in Potential Aerodynamics", Ed. by Morino, Springer-Verlag.

KOCUREK J.D., TANGLER J.L. (1977), Prescribed wake lifting surface hover performance analysis, J. of the American Helicopter Society, Vol.22, N.1, pp.24-35.

LANDGREBE A.J., CHENEY M.C. (1972), Rotor Wakes - Key to Performance Prediction, AGARD-CP-111.

LESIEUR M. (1987), Turbulence in fluids, stochastic and numerical modelling, Martinus Nijhoff Publishers, Dordrecht.

LIEPMANN H.W., LAUFER J. (1947), Investigation of free turbulent mixing, NACA TN 1257.

MOOK D.T. (1988), Unsteady aerodynamics, VKI L.S. 1988-07.

OSTER D., WYGNANSKI I. (1982), The forced mixing layer between parallel streams, J.Fl. Mech., Vol.23, pp. 91-130.

ROSEN A., GRABER A. (1988), Free wake model of hovering rotors having straight or curved blades, J.of the American Helicopter Society, Vol.30, N.3, pp.11-19.

SUMMA J.M., MASKEW B. (1981), A surface singularity method for rotors in hover or climb, USA AVRADCOM-TR-81-D23.

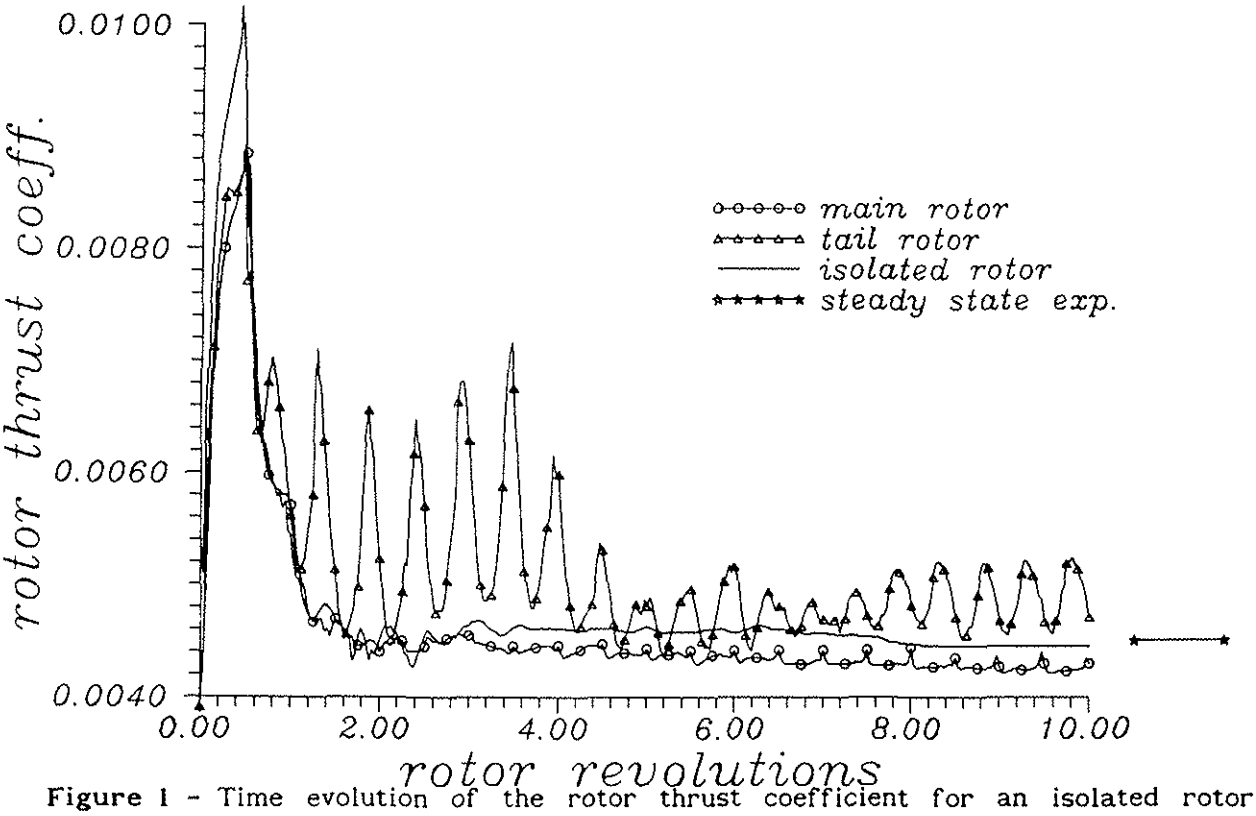

Figure 1 - Time evolution of the rotor thrust coefficient for an isolated rotor and for a main rotor/tail rotor configuration. Impulsive start in hover flight. Experimental steady state data for the isolated rotor by Caradonna and Tung (1981).

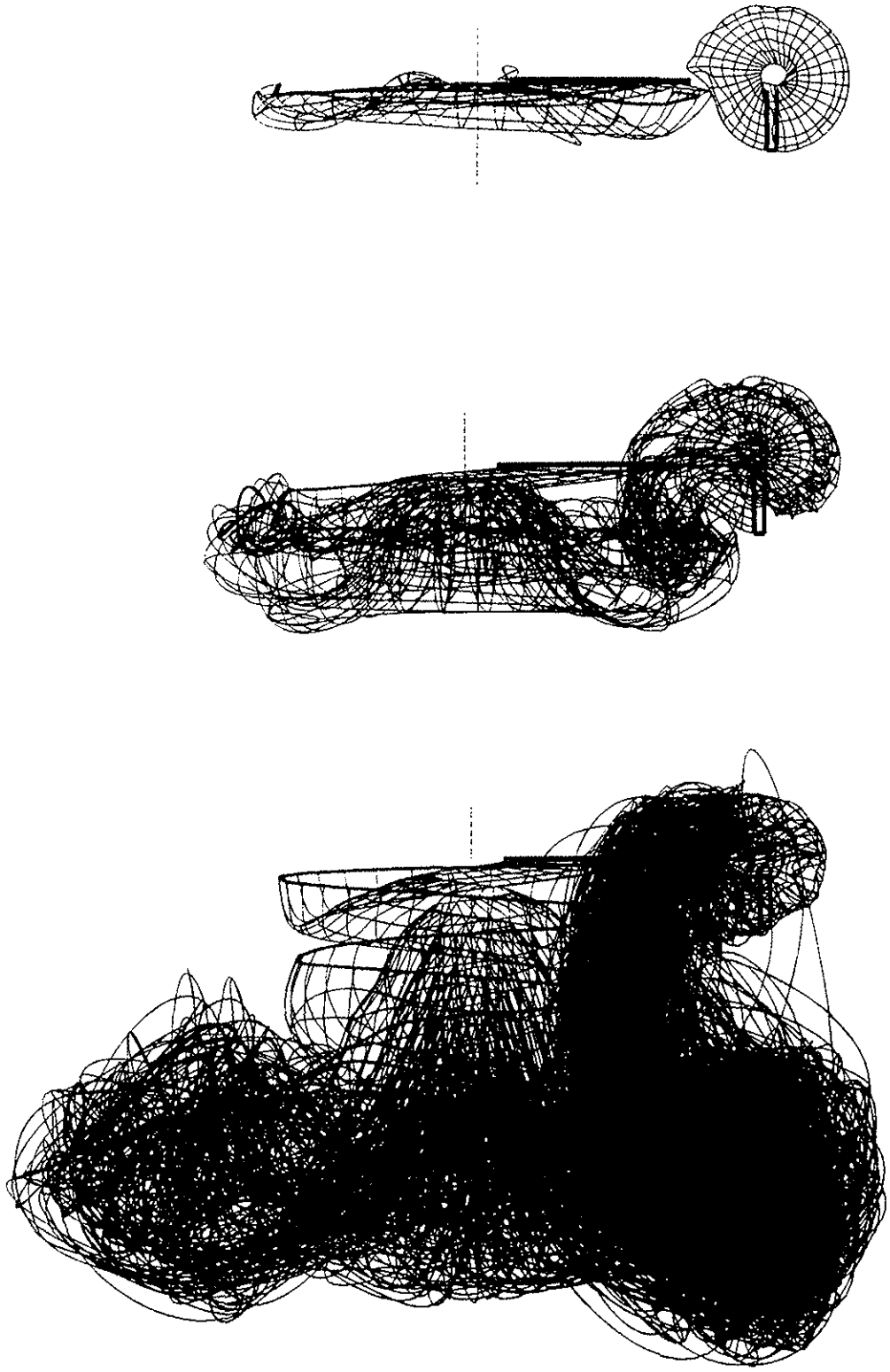

Figure 2 - Time evolution of the wake for a main rotor/tail rotor configuration, after 1, 3 and 10 rotor revolutions. Impulsive start in hover flight. Line thickness proportional to vortex strenght. Dx=1.4R

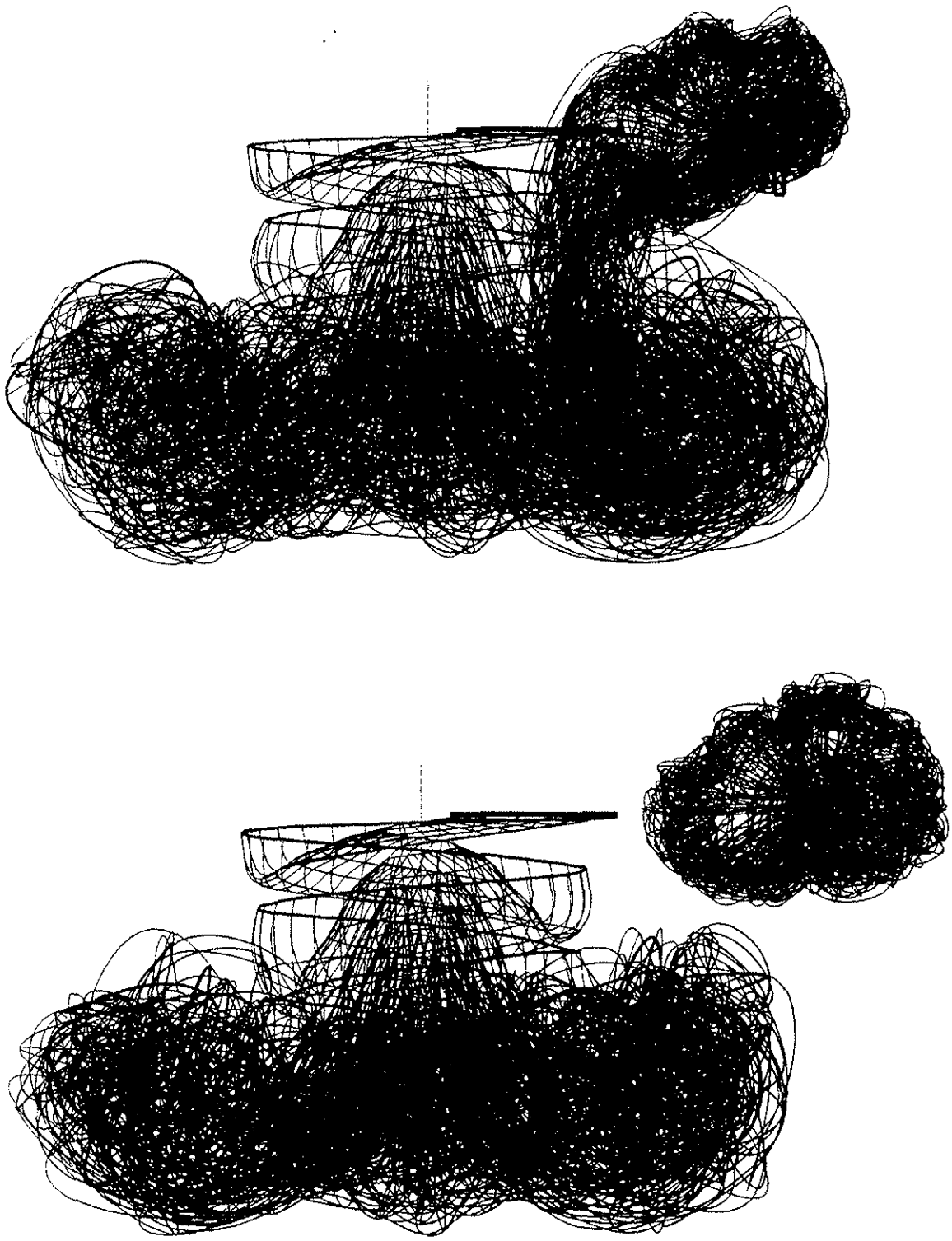

Figure 3 - Configuration of the wake for main rotor/tail rotor configurations, with Dx=1.8R (top) and Dx=2.2R (bottom), after 10 rotor revolutions. Impulsive start in hover flight. Line thickness proportional to vortex strenght.

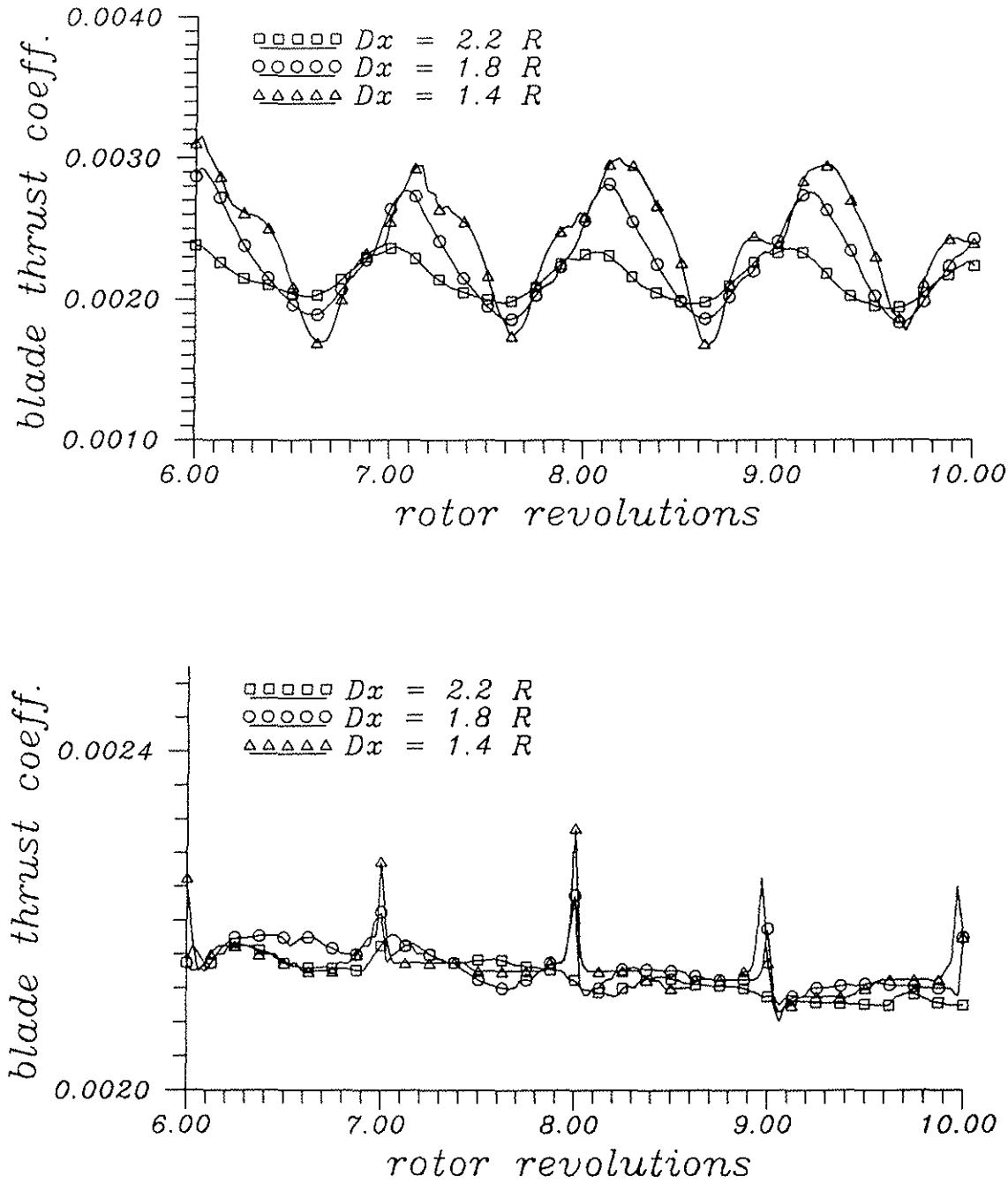

Figure 4 - Instantaneous blade thrust coefficient for main rotor/tail rotor configurations, as a function of the rotor axes separation distance Dx. Approximately steady state hover flight. Tail rotor blade (top) and main rotor blade (bottom).

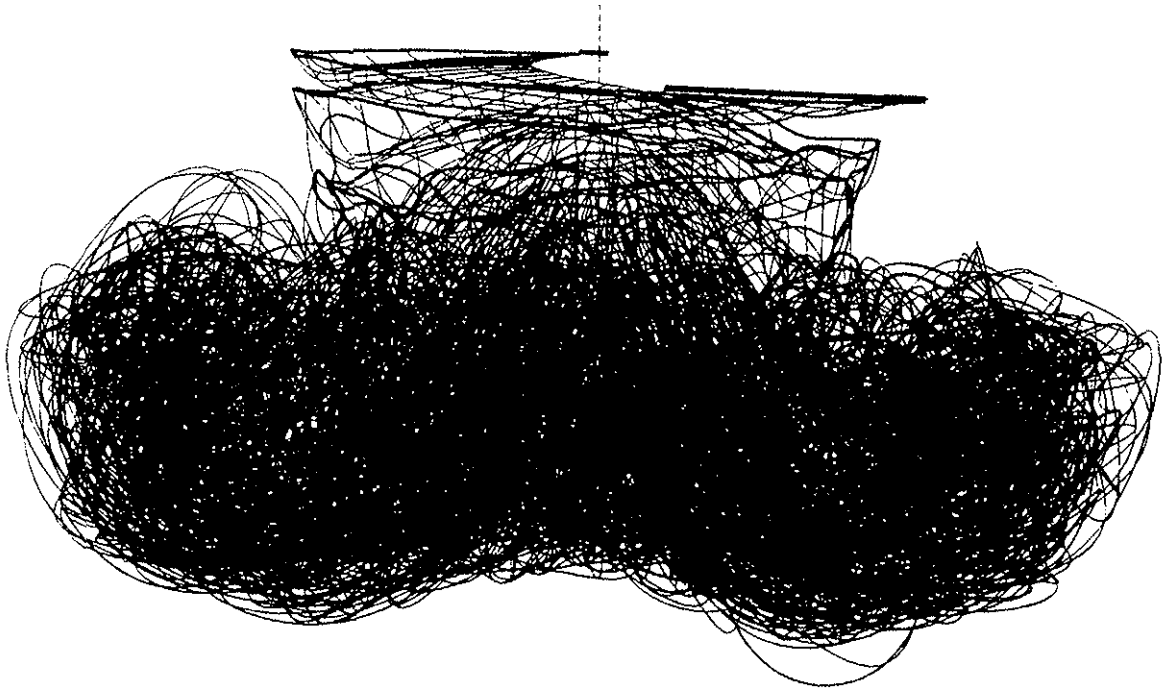

Figure 5 - Configuration of the wake for two coaxial rotors (Dz=0.1R), 8 rotor revolutions after the impulsive start in hover.

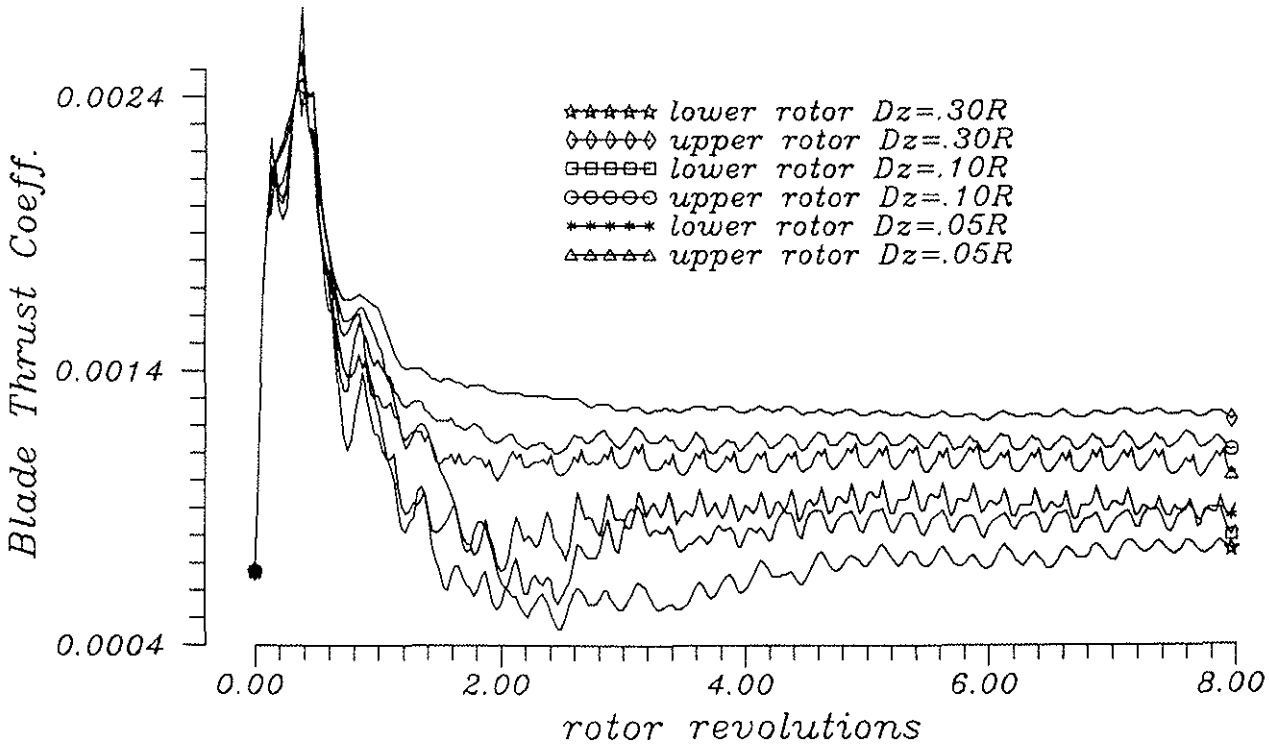

Figure 6 - Time evolution of the thrust coefficient for the blades of the upper and lower rotor, as a function of the vertical separation Dz of the rotor disk planes.

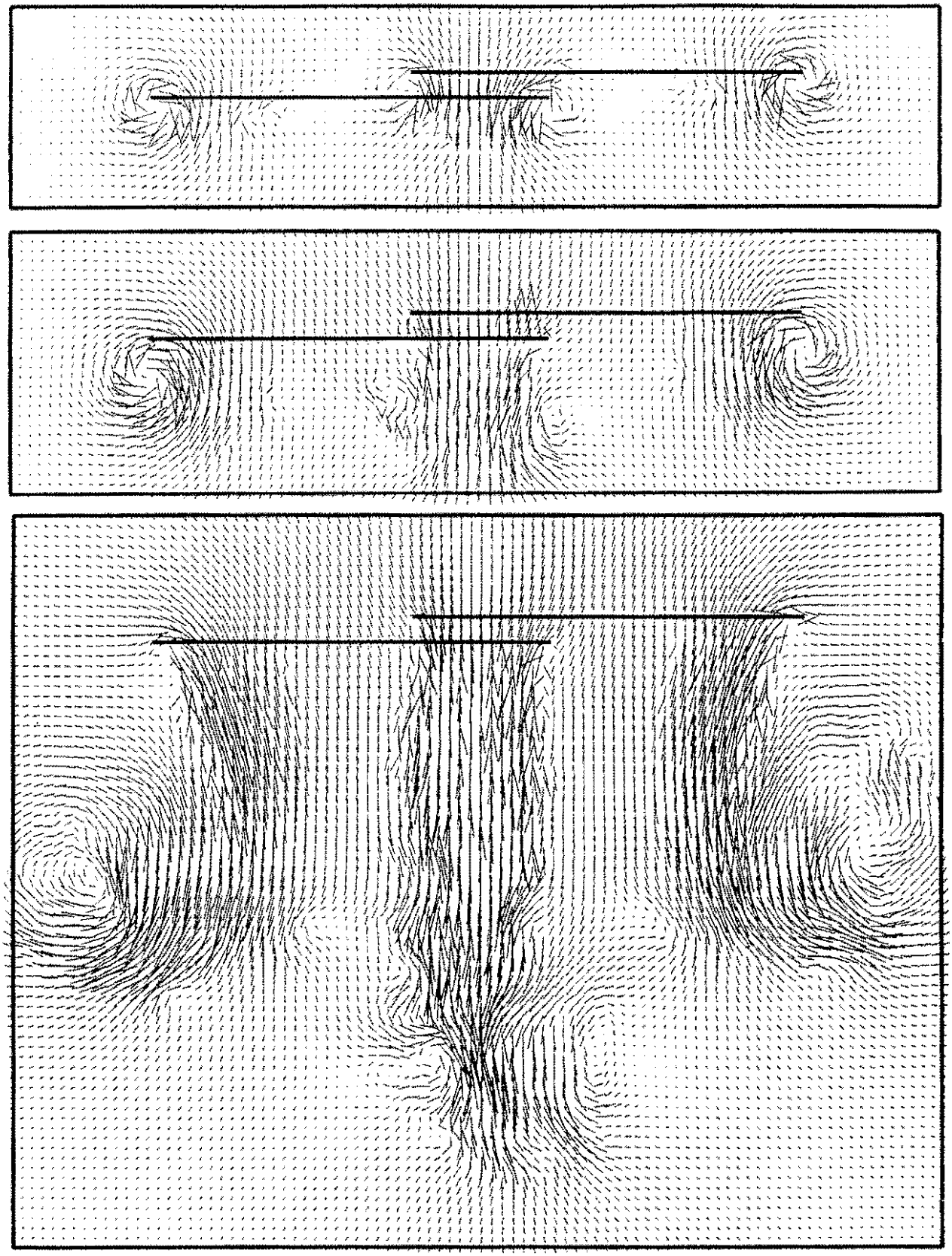

Figure 7 - 2-D vector plot of the instantaneous velocity field in a plane containing the rotor axes of a tandem configuration, 1, 3 and 10 rotor revolutions after the impulsive start in hover.

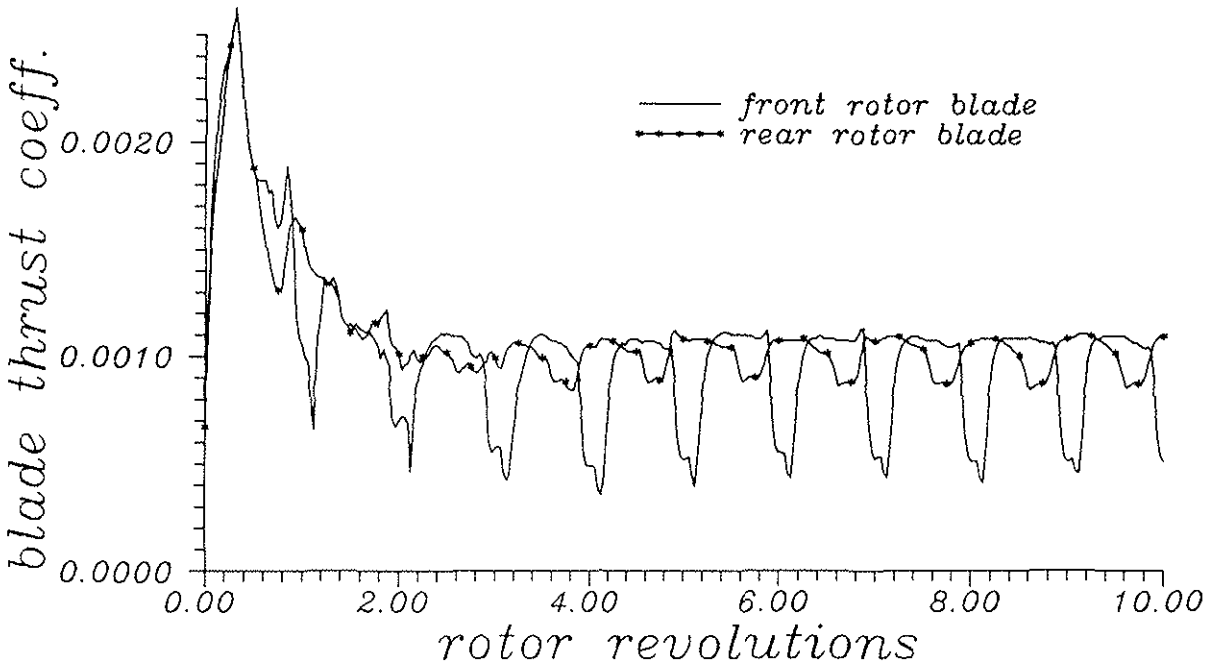

Figure 8 - Time evolution of the thrust coefficient of a single blade of the front and rear rotors of a tandem configuration (Dx=1.3R, Dz=0.13R).